Environ. Res. Lett. **3** (2008) 025005 (7pp) doi:10.1088/1748-9326/3/2/025005

The Explicit-Cloud Parameterized-Pollutant hybrid approach for aerosol–cloud interactions in multiscale modeling framework models: tracer transport results

William I Gustafson Jr, Larry K Berg, Richard C Easter and Steven J Ghan

Atmospheric Science and Global Change Division, Pacific Northwest National Laboratory, PO Box 999, MSIN K9-30, Richland, WA, USA

E-mail: William.Gustafson@pnl.gov

Received 23 January 2008
Accepted for publication 17 March 2008
Published 30 May 2008
Online at stacks.iop.org/ERL/3/025005

Abstract

All estimates of aerosol indirect effects on the global energy balance have either completely neglected the influence of aerosol on convective clouds or treated the influence in a highly parameterized manner. Embedding cloud-resolving models (CRMs) within each grid cell of a global model provides a multiscale modeling framework for treating both the influence of aerosols on convective as well as stratiform clouds and the influence of clouds on the aerosol, but treating the interactions explicitly by simulating all aerosol processes in the CRM is computationally prohibitive. An alternate approach is to use horizontal statistics (e.g., cloud mass flux, cloud fraction, and precipitation) from the CRM simulation to drive a single-column parameterization of cloud effects on the aerosol and then use the aerosol profile to simulate aerosol effects on clouds within the CRM. Here, we present results from the first component of the Explicit-Cloud Parameterized-Pollutant parameterization to be developed, which handles vertical transport of tracers by clouds. A CRM with explicit tracer transport serves as a benchmark. We show that this parameterization, driven by the CRM's cloud mass fluxes, reproduces the CRM tracer transport significantly better than a single-column model that uses a conventional convective cloud parameterization.

Keywords: aerosols, clouds, global climate modeling

1. Introduction

Aerosol–cloud interactions occur on multiple scales of motion and involve a myriad of physical processes that determine the unique characteristics of both the aerosols and clouds. These interactions, if represented at all, are poorly resolved by global climate models (GCM). Typical GCM grid spacings are hundreds of kilometres, whereas convective clouds have diameters ten's of kilometres or less. A typical GCM timestep is 20 min, which is a substantial portion of a convective cloud's lifetime. However, accurately reproducing the impact of the aerosols and clouds is critical for accurately simulating climate. Unlike the ubiquitous greenhouse gases, which have long lifetimes leading to well mixed distributions throughout the atmosphere, aerosols have atmospheric lifetimes on the order of days. This results in a heterogeneous aerosol distribution throughout the globe with higher concentrations near source regions. This also results in regionalized climatological impacts that are more difficult to reproduce in GCMs.

Aerosols are important for climate because of their radiative impact as well as their ability to form cloud condensation and ice nuclei. Aerosol particles scatter and absorb radiation, altering the radiation budget of the atmosphere (the direct effect) (Atwater 1970, Charlson and Pilat 1969, McCormic and Ludwig 1967, Mitchell 1971). The shape and hygroscopic properties of the aerosol particles determine their ability to activate into cloud droplets, which determines the number of cloud and ice droplets within clouds. For more polluted areas with higher aerosol number concentrations, clouds typically form with higher cloud droplet numbers than in pristine areas. Higher droplet numbers lead to a more reflective cloud (the first indirect effect) (Twomey 1991) and can alter the cloud lifetime and precipitation through increased competition for water vapor as droplets grow (the second indirect effect) (Albrecht 1989).

In addition to the aerosol effects on clouds, cloud effects on aerosols must also be reproduced. These effects include nonlinear processes such as convective cloud vertical transport, precipitation scavenging, humidification effects, and aqueous chemistry. Because each of these aerosol and cloud processes involves interactions between the aerosols and meteorology, accurate handling of them requires integrated models with full coupling between the chemistry-aerosol and physics-meteorology portions of the model.

A technique intended to improve the handling of clouds in GCMs is the multiscale modeling framework (MMF), also known as superparameterization or the Cloud-Resolving Convection Parameterization (Grabowski 2001, Randall *et al* 2003). This technique replaces the cloud and radiation parameterizations typically used in a GCM with an embedded cloud-resolving model (CRM) that explicitly simulates the cloud field and parameterizes the radiation at the cloud scale. The CRMs can either be 2D or 3D and can either be independent within each GCM column or linked to neighboring columns as discussed in Randall *et al* (2003).

To date, an MMF model with a prognostic treatment of aerosols has not been developed, primarily due to the additional cost of interactively simulating aerosols within a model that already taxes current computational capabilities. Ideally, since the aerosols and clouds interact at the cloud scale, the aerosols would be embedded with the CRM models within the MMF. The aerosols would be advected within the CRM grids along with parameterizations of the aerosol–climate impacts. However, performing multi-year simulations with this methodology will be too expensive for even the largest computers for the next couple decades. Alternatively, the aerosols could reside and be advected on the coarser GCM grid. Gustafson *et al* (2007) show that neglecting the horizontal variability of aerosols on sub-GCM scales introduces only modest biases in the shortwave cloud forcing. Therefore, one could parameterize interactions between the clouds in the CRMs and the aerosols on the coarse grid. This is the technique employed by the Explicit-Cloud Parameterized-Pollutant (ECPP) parameterization presented in this letter.

This letter presents an overview of ECPP and initial promising results. A detailed description is given for how ECPP parameterizes vertical transport of trace species by convective clouds. This is followed by results showing how ECPP, implemented in a single-column model (SCM), improves the vertical tracer transport. This SCM serves as a proxy for a GCM column within the MMF where ECPP is ultimately designed to be used. Development of ECPP continues, and results showing how ECPP improves aerosol transformation and cloud processing, through processes such as wet scavenging and aqueous chemistry, will be presented in a future paper.

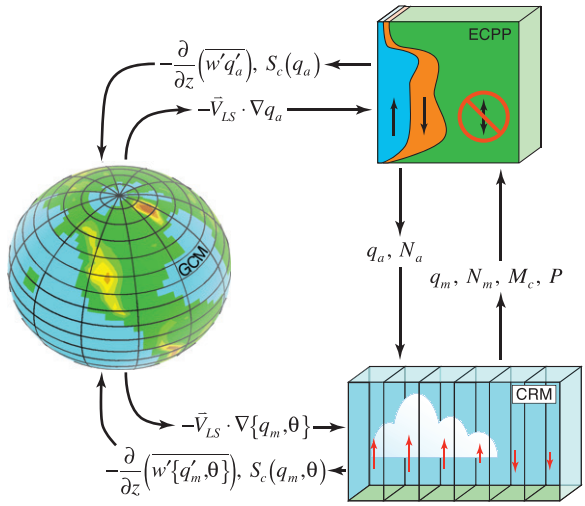

Figure 1. Schematic depiction of ECPP showing linkages between ECPP in relation to the host GCM and embedded CRM's in the MMF. Large-scale advective tendencies of tracer species (subscript a), moisture species (subscript m), and temperature (θ) are provided by the GCM to ECPP and the CRM. ECPP and the CRM exchange information on mass (q), number (N), cloud mass flux (M_c), and precipitation (P), which among other things, are used to determine fractions of area within the GCM column that are assigned to updraft, downdraft, and quiescent draft classes by level. In turn, ECPP and the CRM provide vertical advection and source–sink terms for sub-GCM scales for tracer species (ECPP) and moisture species and temperature (CRM), which are returned to the GCM.

2. Description of ECPP

ECPP acts as an intermediary between the GCM and CRMs within the MMF for processes involving both clouds and trace species, as shown schematically in figure 1. (In this context, trace species include aerosols, trace gases, and inert tracers, which we subsequently refer to as 'tracers'.) For the simplest case of inert tracers, large-scale transport of the tracers occurs within the GCM. The resulting tracer distributions are passed to ECPP where information from the CRMs is used to better simulate cloud-scale vertical transport. A more complex version of ECPP also parameterizes cloud processing of aerosols and trace gases (activation/nucleation, aqueous chemistry, and precipitation scavenging) using cloud/precipitation from the CRMs. The CRMs in turn use aerosol profiles from ECPP to simulate aerosol direct and indirect effects. This letter presents the methodology used to improve the vertical tracer transport. A follow-on paper will address the cloud processing of aerosols and aerosol effects on clouds.

The vertical transport of tracers within ECPP is represented using the cloud mass flux (e.g. Albrecht 1979). The entrainment and detrainment rates used in ECPP are obtained explicitly from the CRM, rather than parameterized as a function of cloud diameter (e.g. Tiedtke 1989, Arakawa and Schubert 1974) for deep clouds, or a constant value (e.g. Siebesma and Holtslag 1996, Siebesma and Cuijpers 1995) for shallow clouds. The first step in ECPP is to categorize each grid cell within the CRM into 'transport classes.' The simplest categorical breakdown is updrafts, downdrafts, and quiescent, where the quiescent class contains cells with small vertical velocities. A more complicated setup could contain multiple updraft and downdraft classes with a series of threshold vertical velocities and/or draft top heights defining the class contents. Tests were performed using the simplest scheme with only one updraft and one downdraft threshold and also a multi-plume scheme with the number of plumes determined by the transport of tracers from each level to the combination of each other level. The more complicated scheme did not substantially improve the performance of the ECPP, so the simplest scheme has been selected to present here.

The updraft and downdraft classes are determined by comparing the vertical velocity in each grid cell with some thresholds. The methodology is similar to that of Greenhut and Khalsa (1982), but is applied over the depth of the atmosphere rather than the planetary boundary layer. The selection of these thresholds is arbitrary, and the methodology presented here attempts to account for characteristics of the updrafts and downdrafts in a realistic way. The first step in computing the thresholds is to determine the root mean squared (RMS) averages of both the upward and downward vertical velocity ($w_{\mathrm{up,RMS}}$ and $w_{\mathrm{down,RMS}}$) at each level of the model. The updraft threshold value is defined as the maximum of 0.1 m s^{-1} or $\alpha_{\mathrm{up}} w_{\mathrm{up,RMS}}$, where α_{up} is an empirically selected constant, set to 1 in this study. The downdraft threshold is similarly defined as the minimum of -0.1 m s^{-1} or $-\alpha_{\mathrm{down}} w_{\mathrm{down,RMS}}$, with α_{down} set to 1 also. This methodology allows for the use of different threshold values for the updrafts and downdrafts, which is consistent with the nature of deep convection with many strong convective updrafts and the generally less vigorous downdrafts. The lower cutoff of 0.1 m s^{-1} is designed for model levels, such as those near the surface or the model top, where the RMS might be quite small. Grid cells that had a vertical velocity greater than the upward threshold, or less than the downward threshold are assigned to be updrafts or downdrafts, respectively.

Once the transport class of each CRM grid cell has been determined (denoted by a subscript j = up, down, or quiescent), the horizontal area fraction, A_j, and the vertical mass flux, M_j, for each transport class are calculated for each level in the CRM. In computing these statistics, CRM variables (e.g., w) are first time-averaged over 20 min intervals, then grid-cell classification and transport-class horizontal averaging is performed. Additional experiments were completed with shorter averaging times, but these results showed somewhat poorer performance.

These profiles are then used to diagnose up- and downdraft entrainment, E_j, and detrainment, D_j, mass flux tendencies using the following formula.

$$\frac{\partial(\rho A_j)}{\partial t} + \frac{\partial M_j}{\partial z} = E_j - D_j \tag{1}$$

ρ, t, and z denote density, time, and height respectively. Note that (1) does not yield a unique expression for E_j and D_j. An assumption similar to that of Arakawa and Schubert (1974) is applied, such that the D_j is zero if M_j increases with altitude, and E_j is zero if the mass flux decreases with altitude. The continuity equation for trace species mixing ratios, $q_{j,L}$, can then be used to solve for the change in tracer mass at each level for each species, L. For the cases of j equals up- and downdraft classes this is:

$$\frac{\partial(\rho A_j q_{j,L})}{\partial t} = -\frac{\partial(M_j q_{j,L})}{\partial z} + (E_j q_{\mathrm{quiescent},L} - D_j q_{j,L}) + S_j \tag{2}$$

where S_j is a source–sink term for the class. And, for the quiescent class:

$$\begin{aligned}\frac{\partial(\rho A_{\mathrm{quiescent}} q_{\mathrm{quiescent},L})}{\partial t} = &-\frac{\partial(M_{\mathrm{quiescent}} q_{\mathrm{quiescent},L})}{\partial z} \\ &+ (D_{\mathrm{up}} q_{\mathrm{up},L} - E_{\mathrm{up}} q_{\mathrm{quiescent},L}) \\ &+ (D_{\mathrm{down}} q_{\mathrm{down},L} - E_{\mathrm{down}} q_{\mathrm{quiescent},L}) + S_{\mathrm{quiescent}}.\end{aligned} \tag{3}$$

Note that the transfer of mass is in opposite directions between (2) and (3), as denoted by the reversed sign on the entrainment minus detrainment terms. Any mass detrained from the quiescent class must be entrained into one of the up- or downdraft classes.

A finite lifetime is assumed for updrafts and downdrafts (two hours in this study), and they are restarted by setting A_{up} and A_{down} to zero every two hours. The individual convective cells in real deep convection also have finite lifetimes. When no lifetime limitation is applied, the ECPP drafts persist for the duration of the convective period (potentially several hours), and weak downdrafts can transport too much material from the mid/upper troposphere to near the surface. For the KWAJEX case used to evaluate ECPP (see next section), organized downdrafts were weak in the CRM simulation. However, there were always some CRM grid cells with downwards vertical velocity during convection periods, and some of them would be classified downdrafts. When no lifetime limitation was applied, the ECPP produced excessive downwards transport of mid-tropospheric tracers, even when a high threshold ($\alpha_{\mathrm{down}} = 4$) was used for downdraft classification. The physically realistic finite-lifetime assumption noticeably improved the ECPP downwards transport in the KWAJEX simulations. We note that identifying organized updrafts and downdrafts using the CRM vertical velocity fields is a difficult problem and an area for continued research.

Most implementations of the mass flux approximation assume steady-state up- and downdrafts. A time-dependent equation for the horizontal-averaged tracer mixing ratio is formed by combining (2) (for j = up and down) and (3), and trace species mixing ratios in updrafts and downdrafts are calculated using steady-state versions of (2). In ECPP, (1)–(3) have been derived to include conditions that are not steady state. The added cost for the time-evolving version is minimal and improves the performance of ECPP in conditions that are not steady state.

3. Evaluation methodology

To make the development and testing of ECPP manageable, an MMF-like testbed has been developed using the chemistry version of the Weather Research and Forecasting model, WRF-Chem (Grell *et al* 2005, Fast *et al* 2006). By running WRF-Chem as a 3D CRM with periodic boundary conditions it is possible to emulate a CRM embedded in a global MMF. The large-scale advection tendencies that would be provided by the GCM are replaced by large-scale forcing tendencies based on field observations. This code and simulation are referred to as WRF-CRM. The relevant statistics that ECPP needs from the CRM are derived from the WRF-CRM run.

A second version of WRF-Chem has been configured to operate as a SCM, with all the physics parameterizations and dynamics removed. In their place, values for state, dynamics, and microphysical variables are obtained from the WRF-CRM run, and ECPP has been inserted to handle the cloud-scale transport and processing of the tracers. This SCM is referred to as WRF-ECPP. The trio of large-scale forcing data, WRF-CRM, and WRF-ECPP collectively act like a single column within the GCM of the MMF. The primary difference between this setup and an actual MMF with ECPP is that the passing of aerosol information from the large-scale (GCM and ECPP) to the cloud-scale (CRM), and treatment of processes whereby aerosols affect clouds, are neglected. For the proof-of-concept purpose presented here, this limitation is acceptable since the tracers are being treated as inert, and aerosol–cloud interactions are uniformly neglected in all of the models (WRF-CRM, WRF-ECPP, and SCAM) applied here.

For comparison with the MMF-like results from WRF-ECPP a simulation is also done using the single-column version of the community atmosphere model (SCAM)(Collins *et al* 2006a, http://www.ccsm.ucar.edu/models/atm-cam/docs/scam). By using the same large-scale forcing dataset for both WRF-CRM and SCAM, one can contrast how a typical GCM (with ∼200 km resolution) handles tracer transport by convective clouds, versus how ECPP improves transport by using mass flux information from the CRM. Since SCAM does not reproduce the same meteorological conditions as WRF-CRM when given the same large-scale forcing, the comparison is not perfect, but as will be shown, a consistent set of behaviors can be identified in each model highlighting the improvements offered by ECPP. SCAM was used in a default setup with the only change being the addition of the inert tracers described below.

The setup used for WRF-CRM is a doubly periodic domain with 122 × 122 × 40 grid points and 2 km horizontal and approximately 0.5 km vertical grid spacing. Large-scale forcing is based on hourly data from 17–31 August 1999 from the Kwajalein Experiment (KWAJEX, e.g. Yuter *et al* 2005) in the Republic of the Marshall Islands. Positive definite advection for cloud/moisture species and inert tracers was used to more accurately conserve mass. The physics parameterizations used are: Thompson microphysics (Thompson *et al* 2008, 2004), CAM longwave and shortwave radiation (Collins *et al* 2006b), YSU boundary layer (Hong *et al* 2006) with a water boundary at the surface, and no cumulus parameterization. Processes affecting the inert tracers in WRF-CRM are grid-resolved advection and turbulent vertical mixing.

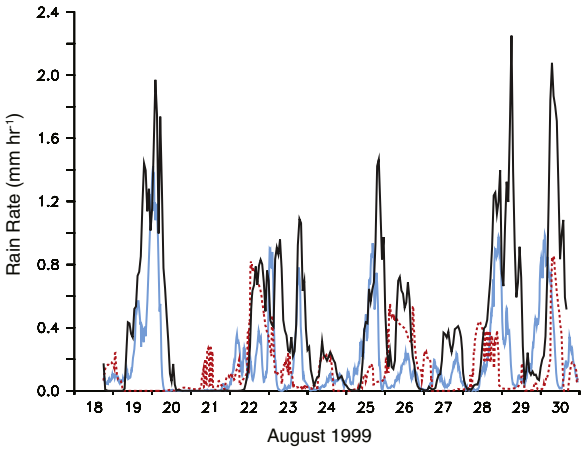

Figure 2. Rain rate time series for University of Washington radar-based observations (blue), WRF-CRM (black), and SCAM (dashed red). Units are mm h^{-1}.

Ten inert tracers have been custom configured in WRF-CRM and SCAM. Each tracer is initialized to a value of 1 ppbv for a 100 hPa deep layer and zero elsewhere: the non-zero values for the bottom tracer extend from the surface to 900 hPa, the next tracer from 900 to 800 hPa, etc, up to the last layer with values from 200 to 100 hPa. Over the course of each day the tracers are transported throughout the domain and then before sunrise, 18 UTC, they are reinitialized to the initial profile for the next day. Both WRF-CRM and SCAM exhibit spin-up behavior during the first day of the run so 18 August 18 UTC is used as the beginning analysis time.

4. Results

First, a comparison of the rain rate time series from WRF-CRM and SCAM versus radar-based estimates from the University of Washington (Houze *et al* 2004) is presented in figure 2. The 12-day mean rain rates are 0.24, 0.43, and 0.17 mm h^{-1} for the observations, WRF-CRM, and SCAM, respectively. While an hour-by-hour match between the models and observations is not necessary for demonstrating the improvements to tracer transport with WRF-ECPP versus SCAM, a general agreement is desired to show the realism of the convective precipitation simulated by the models. Note that ECPP itself does not simulate precipitation, but always uses the microphysical fields from the CRM (WRF-CRM in this test, or MMF-CRM in an actual MMF) with some horizontal and temporal averaging. While the WRF-CRM over estimates the mean rate and some peak rain rates, it does a good job reproducing the episodic nature of the convection. SCAM did not do as well with the timing and under estimates the mean and peak rain rates. However, the SCAM rain rate magnitude is consistent with the observations for the more common rates below 0.5 mm h^{-1}. In addition to model validation, the precipitation time series demonstrate the variety of conditions present during the simulation period. These range from dry

conditions to heavy rain, with the vertical transport varying substantially as a result. The main rationale for an MMF is that its CRMs can better simulate clouds and precipitation than traditional GCM parameterizations, and the somewhat improved rainfall simulation by WRF-CRM versus SCAM reflects this premise. Note that the inclusion of ECPP in an MMF is not expected to produce major changes in the clouds and precipitation simulated by the CRMs. Rather, ECPP should improve the aerosol fields, which will produce modest improvements in some aspects of the simulated clouds and precipitation.

The results for two of the tracers are discussed here. The first tracer is a low-level tracer, released between the surface and 900 hPa. This tracer was selected to allow for the quantification of upward transport from the planetary boundary layer. The other is a high-level tracer, released between 500 and 400 hPa, which was selected to represent the downward transport.

To compare the results from the simulations, and to remove the day-to-day dependence of the simulations, each day in the simulations has been grouped into one of three classes: deep, shallow, and no convection. In order for a day to be classified as having shallow convection or no convection, less than 0.01 ppbv of the low-level tracer could be found within the layer between 400 and 200 hPa at 12 UTC. This measure reflects the net tracer transport between when the profiles were reset at 18 UTC (6 LST) and the analysis time at 12 UTC (midnight local), and is therefore not highly sensitive to the particular hour chosen as long as the period is long enough to capture a sufficient amount of tracer transport. The entire day has not been used because this increased the instances where both deep and shallow convection occur on the same day. Although there were daily differences in the depth of the convection and the amount of precipitation, the simulated convection generally followed a diurnal cycle, and selecting 12 UTC provides representative samples. The majority of the days in the study period had deep convection, but three days in the WRF-CRM simulations and five days in the SCAM simulations were classified as cases of shallow convection, and two days in each simulation had no convection. Note that the tracer profiles presented in figure 3 also reflect the net tracer transport results between 18 and 12 UTC to be consistent with the compositing technique.

There was generally good agreement between the low-level tracer concentration predicted by WRF-CRM and WRF-ECPP (figures 3(c) and (d)). In the cases of deep convection, WRF-ECPP deposits low-altitude tracer over the full depth of the convection. In contrast, SCAM deposits the tracer in two layers, one near 500 hPa, and a broader one near 250 hPa with very little detrainment at other heights. SCAM also leaves significantly more tracer in the injection level. In cases with shallow convection, WRF-CRM and WRF-ECPP loft more low-level tracer into the layer between 900 and 500 hPa compared to SCAM. The thickness of the simulated cloud layer is one reason for this behavior. In all but one case, the tops of the SCAM shallow clouds are less then 700 hPa, while the shallow clouds in WRF-CRM reach as high as 500–400 hPa.

Comparisons were also made for the transport of the high-level tracer. For the deep convection case, WRF-CRM and WRF-ECPP both move the high-level tracer down towards the surface and upwards towards the tropopause, but the agreement is not as good as for the low-level tracer. WRF-ECPP mixes too little tracer over moderate depths (within 200 hPa of the injection level) and too much tracer below 800 hPa. Also, the peak value high-level tracer predicted by WRF-ECPP and SCAM is larger than that simulated by WRF-CRM. Some of this difference can be attributed to the gentle settling of the tracer in the WRF-CRM simulation. In some instances, the convective downdrafts in the WRF-CRM are weak, and downwards transport is dominated by weak compensating subsidence. This subsidence slowly moves the peak high-level tracer values downward, by different amounts on different days, which leads to a smearing of the average tracer profile for WRF-CRM. Similar to the results for the low-level tracer, SCAM leaves too much high-level tracer in the injection level. For the shallow convection case, all three models show very limited transport of the high-level tracer except in the immediate vicinity of the injection level.

The results from WRF-CRM show some day-to-day variability, as shown by the standard deviation indicated in figure 3. In cases with deep convection, the largest variability of the low-level tracer in the WRF-CRM simulations is between 500 and 250 hPa, and is likely related to day-to-day variation of the cloud top. Similarly, the variation of the high-level tracer is also greatest at the higher levels. The behavior of WRF-ECPP is consistent with WRF-CRM, although the variability is slightly less than that simulated by WRF-CRM. SCAM shows much greater variability than WRF-CRM at high levels during instances of deep convection. In cases with shallow convection, the variability in the WRF-CRM and WRF-ECPP simulations is quite small for both the low-level and high-level tracer (only three days were categorized as shallow convection). The variability in the SCAM simulations for shallow convection was also small for the high-level tracer, but was much larger between 900 and 800 hPa for the low-level tracer. This variability is likely related to day-to-day differences in the SCAM simulated shallow clouds.

As a metric to evaluate the performance of each method, the normalized root mean squared error (RMSE) has been computed for WRF-ECPP and SCAM during cases with deep and shallow convection. WRF-CRM is used as the control for comparison, and the normalization is done at each time using the mean profile value, roughly 0.1 ppbv. Before these calculations could be completed each simulation was interpolated to 100 hPa intervals to minimize bias towards the WRF model levels. The WRF-ECPP RMSE is between a factor of 1.5 and 2 smaller then the SCAM RMSE in each case (table 1). The relatively coarse resolution of SCAM and the amount of numerical diffusion associated with each model resolution likely affects the RMSE results.

5. Conclusions

A new methodology for representing the cloud-scale transport and transformation of aerosols and trace gases in MMF models is introduced. This new Explicit-Cloud Parameterized-Pollutant (ECPP) parameterization is designed to represent im-

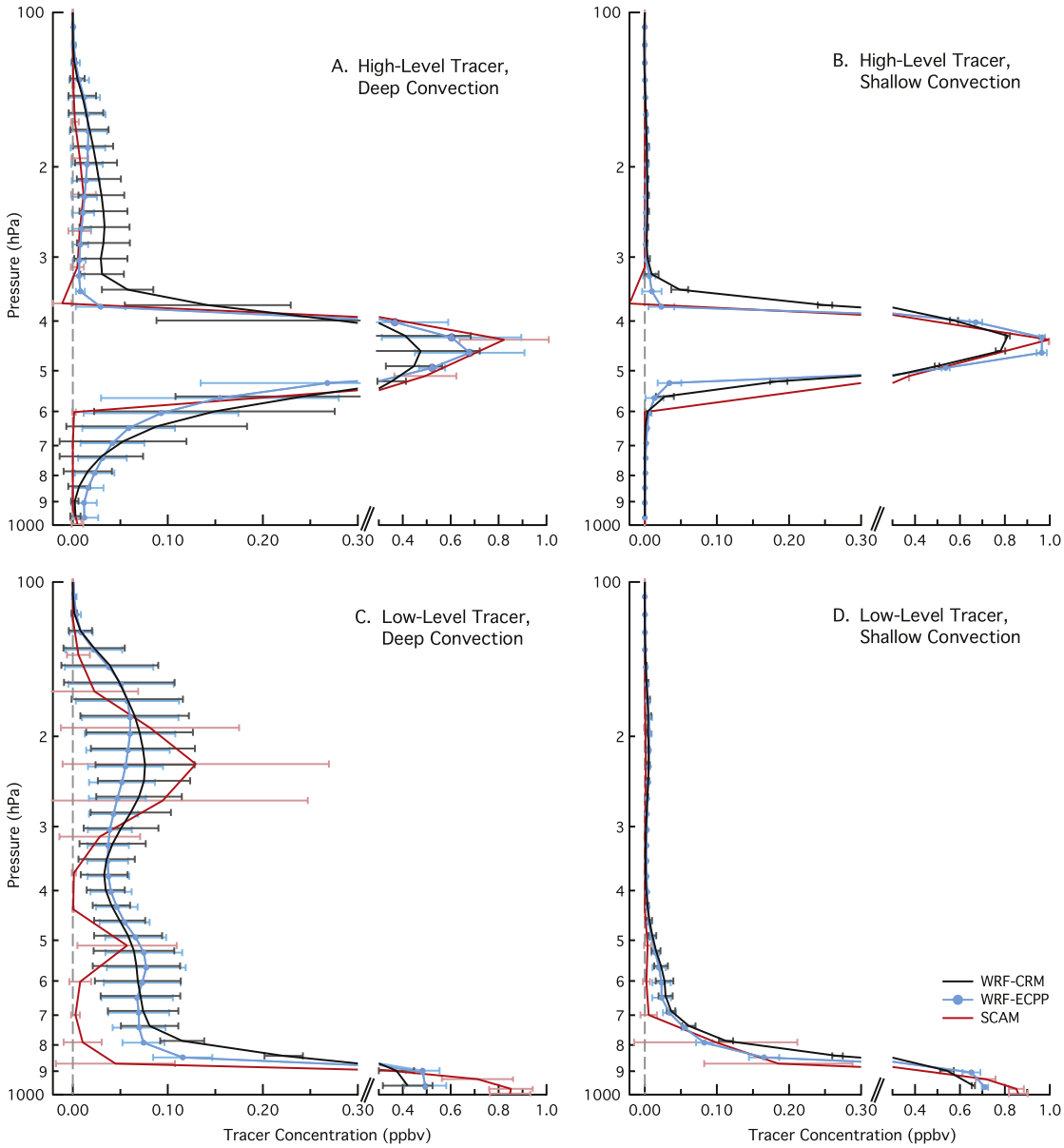

Figure 3. Tracer concentration for WRF-CRM (black), WRF-ECPP (blue), and SCAM (red) for cases with both a high-level tracer and deep convection (A) and shallow convection (B); and a low-level tracer for cases with deep convection (C), and shallow convection (D). The values represent composited profiles at 12 UTC, as described in the text. The horizontal bars indicate the standard deviation between the days within the composite. Note the split horizontal axes for clarity outside of the tracer injection level. Also, a minor adjustment to the vertical levels was done to aid in differentiating overlapping standard deviation bars.

portant cloud–aerosol interaction processes within convective clouds.

This study focuses on the transport of passive tracers by convective clouds. WRF-Chem is applied as a three-dimensional CRM to simulate a 13-day period from KWAJEX. The updraft and downdraft statistics are used in a single-column version of WRF (WRF-ECPP) to represent the transport of passive tracers. Tracer transport is also simulated with the CAM single-column model, which has a traditional parameterization of convective cloud transport. The WRF-CRM tracer transport results are then used to evaluate the WRF-ECPP and SCAM results.

In this study, there is better agreement between the tracer profiles simulated with WRF-CRM and with WRF-ECPP than with the tracer profiles obtained with SCAM. Similar to the results from WRF-CRM, WRF-ECPP is able to deposit both representative low-level and high-level tracers over a wide

Table 1. Normalized RMSE of high-level and low-level tracer concentrations simulated with WRF-ECPP and SCAM separated by cases with deep convection and shallow convection. The simulations are interpolated to 100 hPa increments for this calculation.

	Deep convection		Shallow convection	
	WRF-ECPP	SCAM	WRF-ECPP	SCAM
High-level tracer	0.375	0.640	0.320	0.643
Low-level tracer	0.448	0.671	0.471	0.721

range of heights. SCAM tends to deposit both tracers in specific layers. The RMSE has been computed for both WRF-ECPP and SCAM, and the RMSE associated with the WRF-ECPP simulations is smaller by a factor of 1.5–2 than the RMSE computed from the SCAM simulations, demonstrating that WRF-ECPP can make a significant improvement in the treatment of the transport of a passive tracer in the MMF.

Further work is needed to extend this approach to other effects of clouds on aerosols, including activation, aqueous chemistry, resuspension, and precipitation scavenging.

Acknowledgments

We wish to thank Mikhail Ovtchinnikov of PNNL and two anonymous reviewers for their insightful reviews of our draft paper, Stacy Brodzik and Robert Houze of the University of Washington for their assistance with the rain rate data, and Vaughn Phillips of Princeton University for the KWAJEX large-scale forcing data. This manuscript has been authored by Battelle Memorial Institute, Pacific Northwest Division, under contract No. DE-AC05-76RL01830 with the US Department of Energy. The United States Government retains and the publisher, by accepting the article for publication, acknowledges that the United States Government retains a non-exclusive, paid-up, irrevocable, world-wide license to publish or reproduce the published form of this manuscript, or allow others to do so, for United States Government purposes. This work was also supported by the NASA Interdisciplinary Science Program under grant NNX07AI56G.

References

Albrecht B A 1979 Model of the thermodynamic structure of the trade-wind boundary-layer. 2. Applications *J. Atmos. Sci.* **36** 90–8

Albrecht B A 1989 Aerosols, cloud microphysics, and fractional cloudiness *Science* **245** 1227–30

Arakawa A and Schubert W H 1974 Interaction of a cumulus cloud ensemble with large-scale environment. 1 *J. Atmos. Sci.* **31** 674–701

Atwater M A 1970 Planetary albedo changes due to aerosols *Science* **170** 64–6

Charlson R J and Pilat M J 1969 Climate: the influence of aerosols *J. Appl. Meteorol.* **8** 1001–2

Collins W D *et al* 2006a The community climate system model version 3 (CCSM3) *J. Clim.* **19** 2122–43

Collins W D, Rasch P J, Boville B A, Hack J J, McCaa J R, Williamson D L, Briegleb B P, Bitz C M, Lin S J and Zhang M H 2006b The formulation and atmospheric simulation of the community atmosphere model version 3 (CAM3) *J. Clim.* **19** 2144–61

Fast J D, Gustafson W I, Easter R C, Zaveri R A, Barnard J C, Chapman E G, Grell G A and Peckham S E 2006 Evolution of ozone, particulates, and aerosol direct radiative forcing in the vicinity of Houston using a fully coupled meteorology-chemistry-aerosol model *J. Geophys. Res.* **111** D21305

Grabowski W W 2001 Coupling cloud processes with the large-scale dynamics using the cloud-resolving convection parameterization (CRCP) *J. Atmos. Sci.* **58** 978–97

Greenhut G K and Khalsa S J S 1982 Updraft and downdraft events in the atmospheric boundary layer over the equatorial Pacific Ocean *J. Atmos. Sci.* **39** 1803–18

Grell G A, Peckham S E, Schmitz R, McKeen S A, Frost G, Skamarock W C and Eder B 2005 Fully coupled 'online' chemistry within the WRF model *Atmos. Environ.* **39** 6957–75

Gustafson W I, Chapman E G, Ghan S J, Easter R C and Fast J D 2007 Impact on modeled cloud characteristics due to simplified treatment of uniform cloud condensation nuclei during NEAQS 2004 *Geophys. Res. Lett.* **34** L19809

Hong S Y, Noh Y and Dudhia J 2006 A new vertical diffusion package with an explicit treatment of entrainment processes *Mon. Weather Rev.* **134** 2318–41

Houze R A, Brodzik S, Schumacher C, Yuter S E and Williams C R 2004 Uncertainties in oceanic radar rain maps at Kwajalein and implications for satellite validation *J. Appl. Meteorol.* **43** 1114–32

McCormic R A and Ludwig J H 1967 Climate modification by atmospheric aerosols *Science* **156** 1358–9

Mitchell J M 1971 The effect of atmospheric aerosols on climate with special reference to temperature near the Earth's surface *J. Appl. Meteorol.* **10** 703–14

Randall D, Khairoutdinov M, Arakawa A and Grabowski W 2003 Breaking the cloud parameterization deadlock *Bull. Amer. Meteorol. Soc.* **84** 1547–64

Siebesma A P and Cuijpers J W M 1995 Evaluation of parametric assumptions for shallow cumulus convection *J. Atmos. Sci.* **52** 650–66

Siebesma A P and Holtslag A A M 1996 Model impacts of entrainment and detrainment rates in shallow cumulus convection *J. Atmos. Sci.* **53** 2354–64

Thompson G, Field P R, Rasmussen R M and Hall W D 2008 Explicit forecasts of winter precipitation using an improved bulk microphysics scheme. Part II: implementation of a new snow parameterization *Mon. Weather Rev.* at press

Thompson G, Rasmussen R M and Manning K 2004 Explicit forecasts of winter precipitation using an improved bulk microphysics scheme. Part I: description and sensitivity analysis *Mon. Weather Rev.* **132** 519–42

Tiedtke M 1989 A comprehensive mass flux scheme for cumulus parameterization in large-scale models *Mon. Weather Rev.* **117** 1779–800

Twomey S 1991 Aerosols, clouds and radiation *Atmos. Environ.* **25** 2435–42

Yuter S E, Houze R A, Smith E A, Wilheit T T and Zipser E 2005 Physical characterization of tropical oceanic convection observed in KWAJEX *J. Appl. Meteorol.* **44** 385–415